Tikrit Journal of Engineering Sciences (2025); 32(4): 2151
DOI: http://doi.org/10.25130/tjes.32.4.15

IRAQI Academic Scientific Journals

ISSN: 1813-162X (Print); 2312-7589 (Online)
Tikrit Journal of Engineering Sciences
available online at: http://www.tj-es.com

TJES Tikrit Journal of Engineering Sciences

A Numerical Study of Uniform Copper Foam Porous Disk Distribution for Heat Transfer Enhancement in Parabolic Trough Collectors

Mustafa F. Hasan *, Mohammed A. Nima
Mechanical Department, Engineering College, Baghdad University, Baghdad, Iraq.

Keywords:
Iraq's Climate, Metal Foam Insert, Parabolic trough collector, Porous Disc.

Highlights:

- *Effect of metal foam inserts on heat transfer in PTC receiver pipes.*
- *Optimized placement of copper foam to enhance heat exchange efficiency.*
- *Simulating solar radiation and flow variations for realistic conditions.*
- *Temperature gradients with and without metal foams in absorber pipes.*

ARTICLE INFO
Article history:

Received	23 Apr. 2024
Received in revised form	12 Aug. 2024
Accepted	06 Nov. 2024
Final Proofreading	26 Aug. 2025
Available online	30 Aug. 2025

Citation: Hasan MF, Nima MA. **A Numerical Study of Uniform Copper Foam Porous Disk Distribution for Heat Transfer Enhancement in Parabolic Trough Collectors**. *Tikrit Journal of Engineering Sciences* 2025; **32**(4): 2151.
http://doi.org/10.25130/tjes.32.4.15

*Corresponding author:
Mustafa F. Hasan
Mechanical Department, Engineering College, Baghdad University, Baghdad, Iraq.

Abstract: A computational study was conducted to examine the possible performance improvement of the thermal efficiency of parabolic trough solar collectors by inserting copper foam blocks inside the receiver tube. Ten discs of evenly distributed metal copper foam blocks were placed along the pipe to facilitate heat exchange. Simulations were conducted under stable, incompressible, and three-dimensional flow conditions. The flow within the copper foam domain of the flow system was described using the Brinkman-Forchheimer model, while the fluid domain was controlled by the Navier-Stokes equation. Thus, the energy equation was used for an accurate prediction of the temperature distribution in the entire continuum of fluid and porous media. This thorough method considered environmental elements like typical levels of solar radiation in Iraq from 9:00 AM to 4:00 PM, along with a flow rate variation of 0.3 to 1.5 LPM for simulation. The results indicated that integrating metal foam decreased absorber plate temperature compared to the scenario without metal foam, resulting in increased collector efficiency. The results indicated a 17% increase in thermal efficiency, indicating significant energy savings and improved practicality of solar energy use in arid areas, such as Iraq. The results also showed that the optimal insertion of metal foam with a 30% filling ratio significantly improved thermal performance, resulting in a 76% improvement in mean heat transfer coefficients. These significant findings underscore how properly planned positioning of metal foams can serve as an effective option for enhancing heat transfer efficiency and outlet temperature regulation in PTSC.

دراسة عددية للتوزيع المنتظم لأقراص رغوة النحاس المسامية الموحدة لتعزيز انتقال الحرارة في مجمعات الطاقة الشمسية ذات الحوض المكافئ

مصطفى فالح حسن، محمد عبد الرؤوف نعمة
قسم الهندسة الميكانيكية/ كلية الهندسة / جامعة بغداد / بغداد – العراق.

الخلاصة
أجريت دراسة حاسوبية لبحث إمكانية تحسين كفاءة الأداء الحراري لمجمعات الطاقة الشمسية ذات القطع المكافئ عن طريق إدخال كتل رغوة النحاس داخل أنبوب المستقبل. تم وضع عشرة أقراص من كتل رغوة النحاس الموزعة بشكل متساوٍ على طول الأنبوب لتسهيل تبادل الحرارة. وبناءً على ذلك، أجريت عمليات المحاكاة تحت ظروف تدفق مستقرة وغير قابلة للانضغاط وثنائية الأبعاد. تم وصف التدفق داخل مجال رغوة النحاس في نظام التدفق باستخدام نموذج برينكمان-فورشهايمر، في حين تم التحكم في مجال السائل بواسطة معادلة نافير-ستوكس. وبالتالي، تم استخدام معادلة الطاقة للتنبؤ الدقيق بتوزيع درجة الحرارة في كل من وسط السائل ووسط المسام. أخذت هذه الطريقة الشاملة بعين الاعتبار العوامل البيئية مثل مستويات الإشعاع الشمسي النموذجية في العراق من الساعة ٩:٠٠ صباحًا حتى ٤:٠٠ مساءً، مع تباين معدل التدفق من ٠,٣ إلى ١,٥ لتر/دقيقة للمحاكاة. أشارت النتائج إلى أن دمج رغوة المعدن أدى إلى انخفاض في درجة حرارة لوحة الامتصاص مقارنة بالسيناريوهات التي لا تحتوي على رغوة معدنية، مما أدى إلى زيادة كفاءة المجمع. تشير النتائج إلى زيادة في الكفاءة الحرارية بنسبة ١٧٪، مما يشير إلى توفير كبير في الطاقة وتحسين جدوى استخدام الطاقة الشمسية في المناطق الجافة مثل العراق. كما أظهرت النتائج أن الإدخال الأمثل لرغوة المعدن بنسبة ملء ٣٠٪ قد حسّن بشكل كبير الأداء الحراري، مما أدى إلى تحسن بنسبة ٧٦٪ في متوسط معاملات نقل الحرارة. أكدت هذه النتائج الهامة أن التخطيط المناسب لوضع رغوة المعدن يمكن أن يكون خيارًا فعالاً لتحسين كفاءة نقل الحرارة وتنظيم درجة حرارة المخرج في مجمعات الطاقة الشمسية ذات القطع المكافئ.

الكلمات الدالة: المناخ العراقي، حشوة الرغوة المعدنية، مجمع القطع المكافئ، القرص المسامي.

1.INTRODUCTION

There is widespread acknowledgment of the need to shift from non-renewable fossil fuels to sustainable energy sources to address environmental concerns, global warming, and escalating energy needs. Solar power has garnered significant attention among alternative energy sources due to its worldwide availability and substantial potential. Various methods have been developed for harnessing inexhaustible solar energy. PTC acts as a linear concentrated solar collector that uses a reflector to direct sunlight into the absorbent tube. In this design, the heat transfer fluid (HTF) ingests thermal energy outside the absorber tube and transfers it via conduction and convection. However, the main challenge in PTC systems is that HTF, like water, is weak radiation soaking. To address this issue, studies have explored various strategies, such as adding nanoparticles to the core heat transfer fluid, employing metal foams, and combining metallic foams with nanofluids. This technology aims to provide increased radiation absorption and improve the overall thermal efficiency of PTC systems. There has been an increased interest in using metallic foams to improve efficiency and increase heat transfer in PTC applications. The adoption of porous materials as the main removal technology results in high levels of flow mixing and a large surface area compared to their volume. Ashby et al. [1] stated that metallic foams are a separate group, and they are used for heat transfer and structural mechanics. Metal foams are produced in two forms: open and closed cell structures. Open-cell copper foam is made from interconnected holes that enable fluid passage, creating channels between adjacent pores. Numerous investigations have explored the enhanced thermal performance of PTC using methods, such as incorporating metal foam. Alkam and Al-Nimr [2] found that the thermic efficiency of a flat-plate solar water collector was enhanced through the integration of circular aluminum foam substrates mounted on the inner walls of the riser. This configuration improved the rate of heat transfer at the riser wall, leading to a notable 27-fold increase in the Nusselt number. Nonetheless, it was observed that incorporating porous substrates led to a substantial rise in pressure drop, reaching up to 32 times its original level. Kumar and Reddy [3, 4] performed computational analyses on absorber pipes outfitted with porous disc inserts. Their study concentrated on examining how the various geometrical properties of the porous disks influenced heat transfer improvement. The results revealed that incorporating porous discs significantly improved heat transfer effectiveness, leading to a more consistent temperature gradient across the absorber tube. Similarly, Mwesigye [5] studied perforated plate inserts in absorber tubes to examine their impact on the rate of heat transfer. The results revealed a marked reduction in both the maximum temperature and temperature fluctuations around the circumference of the absorber tube when these inserts were employed. Wang et al. [6] explored the thermal-fluid dynamics characteristics of a PTC pipe that was partially filled with copper foam. When the dimensional height of the copper foam, expressed as a ratio to the tube diameter, was 0.25, both the Nusselt number and friction factor showed substantial increases compared to those of an unfilled tube by 10 and 20 fold, respectively. Zheng et al. [7] examined the properties of vapor and heat transfer and flow in a partially with metal foam occupied PTC pipe with varying levels of porosity, i.e., from 0.951 to 0.975. The results revealed an enhancement in the Nusselt number, i.e.,

increased by 16 times, and a corresponding increase in the friction factor, i.e., increased by 253 times. Jamal-Abad et al. [8] investigated the thermal and fluid performance of the PTR tube with 90% porosity and copper foam with a pore density of 30 PPI. The results showed a significant increase in the Nusselt number by 73.4% and a significant increase in the friction factor of 130 times. Heyhat et al. [9] experimentally determined the optimal temperature of absorption PTC. The receiver pipe contained copper metal foam and cupric oxide acting as a nanofluid in a laminar flow. The findings showed that the use of foam resulted in a 26% increase in thermal efficiency. Valizade et al. [10] investigated the effect of using metal foam to enhance heat transfer on PTC performance. They found an increase of 171.2% and 119.6% for fully porous and semi-porous systems, respectively. Peng et al. [11] numerically examined the impact of gradient metal foam inserted within a PTC receiver pipe. Gradient metal foam increased the Nusselt number by 43.7-812.6%. Peng et al. [12] conducted both an experimental and computational analysis to determine the impact of utilizing porous fins at the receiver pipe's bottom on a parabolic collector's performance. The Nusselt number increased by 256.3–838%, which was one of the noteworthy outcomes. Helmi et al. [13] investigated the effectiveness of solar collectors with parabolic rotating troughs using a computer model that combined magnetic nanofluids and porous fins. According to the investigation, the receiver pipe with copper porous fins and a porosity of 0.97 had a 3.7-fold higher heat transfer rate than an empty receiver. Within a numerical investigation, Esmaeili et al. [14] enhanced a PTC's performance by combining creative turbulators and hybrid nanofluids. The study found that heat transmission increased by 35.7%. Heyhat and Khattar [15] experimentally investigated the impact of various metal foam shapes on the direct absorption of PTC's thermal performance in the laminar flow. The study's findings demonstrated that, at 50.8%, the receiver pipe with porous foam inside generated the highest thermal efficiency. Esmaeili et al. [16] investigated the effect of metal foam on PTCs' thermal performance through an experimental study. Three foam configurations inside the receiver pipe were examined. The results showed that the periodic array configuration of metal foams produced the highest improvement in thermal efficiency, with a 14% rise over a pipe without a porous medium. Farhan et al. [17] studied the thermal performance of a compound parabolic collector (CPC) receiver with unevenly spaced copper metal foam inserts. Experimental and numerical evaluations were conducted on PPI10 and PPI20 foams of varied thicknesses. The results indicated that PPI20 foam improved heat transfer more than PPI10; however, it also increased pressure drops. PPI20 had the highest performance at lower flow rates. The gradual dispersion of metal foam enhanced heat transfer while minimizing pressure drops, providing a new design for maximizing CPC efficiency. This study helps to understand how uneven metal foam distribution might improve solar collector performance while minimizing pressure drop. Several studies have emphasized the need to achieve optimal heat transfer and flow efficiency when utilizing MFI in PTC pipes. Overcoming this issue is critical to increasing the thermal efficiency of PTC systems. The use of a partially embedded MFI appears to be a promising method for reducing flow velocity and enhancing the temperature gradient. Under these conditions, the metal foam contributes to the balance by reducing net field strength and pore leakage. Ashsai. [18] and Lee et al. [19] both confirmed the efficacy of this technique. Moreover, the non-uniform transfer of heat in the PTC has a substantial impact on heat flow performance, leading to a variable temperature distribution in the PTC pipe. Addressing these differences is essential for measuring the thermal efficiency of a PTC fluid with MFI, especially compared to foamless tubes in scenarios of steady heat flow. The present study investigates how heat is transferred and fluids move within a PTC pipe utilizing MFI and water. Temperature changes around the absorber tube are a common cause of poor heat distribution and reduced performance in PTC systems. The study examined how changing radiation levels from 500 to 900 W/m² and fluid flow rates from 0.3 to 1.5 LPM impacted heat transfer. The algorithm will predict isotherms, streamlines, and thermal behavior in the PTC pipe, as well as estimate heat transfer coefficients to assess efficiency. The present study examines the effect of different metal foam layouts on absorber pipes on circumferential temperature gradients by comparing setups without metal foam to those with complete metal foam installations. The present study aims to understand better how metal foam can be used in PTC pipes to improve thermal efficiency. The findings will aid in improving knowledge of thermal-hydraulic performance in PTC systems, allowing for improved design options for solar energy collectors.

2.MATHEMATICAL FORMULATION

2.1.Physical Configuration

Figure 1 shows the PTC setup, which consists of a pipe receiver and a PTC. The PTC absorbs the sunlight reflected by the PTC and converts it to energy. Copper foam discs were partially filled in a PTC pipe. The foam blocks, positioned radially along the pipe, have a pore density of

40 PPI and a porosity of 0.8981. Ten discs are uniformly distributed in total: one at the inlet, eight spaced evenly along its length, and one at the exit. The dimensions of the tube were as follows: length of 1.5 m, outer diameter of 28 mm, and inner diameter of 26 mm, resembling those used in previous thermal-hydraulic studies. Water serves as an appropriate operating fluid due to its constancy and wide temperature range.

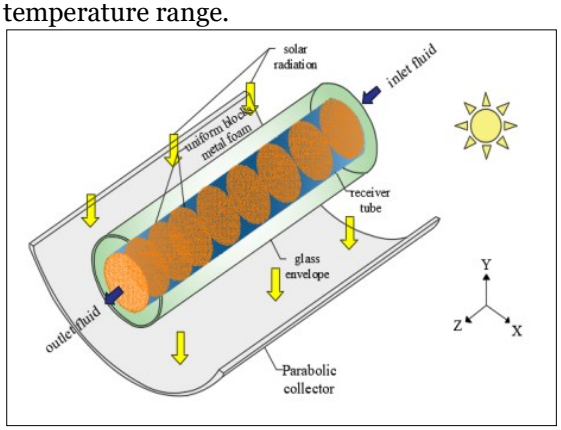

Fig. 1 Schematic Diagram of the Physical Domain.

2.2.Presumptions

Certain assumptions must be considered to simplify the flow and heat transfer equations, which involve conservation of mass, momentum, and energy:

1) Flow is continuous, smooth, and in a non-compressible manner.
2) Absorption pipe with a smooth surface and wall that prevents slipping.
3) The effects of heat production and dissipation are not considered.
4) The porous material is strong, uniform, equally effective in all directions, and thoroughly soaked with water.
5) Both solid and fluid components have similar properties throughout.
6) Buoyancy's impact is taken into account using Boussinesq's approximation method.
7) Radiant heat transfer between surfaces and inside the absorber pipe was ignored.

2.3.Formula Mathematical Governance

The present study used the Navier-Stokes equation to investigate the flow field in a transparent fluid region and the Brinkman-Forchheimer model to depict the flow field in a porous medium. To portray heat activity in the MFI, it is assumed that LTE exists in both the solid and fluid parts. The equations presented were based on work from [20]:

(1) Continuity equation:

$$\frac{\partial}{\partial xi}\left(\rho_f u_i\right) = 0 \qquad (1)$$

where cursive f refers to HTF, ρ is the density, and u_i is the direction of motion in $x, y,$ or z.

(2) Momentum Formula:

(2.1) Zone non porous:

$$\frac{\partial}{\partial x_j}\left(\rho_f u_i u_j\right) = -\frac{\partial p_i}{\partial x} + \frac{\partial}{\partial x_j}\left[(\mu + \mu_t)\left(\frac{\partial u_i}{\partial x_j} + \frac{\partial u_j}{\partial x_i}\right) - \frac{2}{3}(\mu + \mu_t)\frac{\partial u_i}{\partial x_i}\delta_{ij}\right] + (\rho\beta)_f(T - T_b)\,\vec{g} \qquad (2)$$

(2.2) Porous region:

$$\frac{1}{\varphi^2}\frac{\partial}{\partial x_j}\left(\rho_f u_i u_j\right) = -\frac{\partial p}{\partial x_i} + \frac{1}{\varphi}\frac{\partial}{\partial x_j}[(\mu + \mu_t)(\frac{\partial u_i}{\partial x_j} + \frac{\partial u_j}{\partial x_i}) - \frac{2}{3}(\mu + \mu_t)\frac{\partial u_i}{\partial x_i}\delta_{ij}] - (\frac{\mu + \mu t}{K}u_i + \frac{\rho F}{\sqrt{K}}|\vec{u}|u_i) + (\rho\beta)_f(T - T_b)\,\vec{g} \qquad (3)$$

(3) Energy Formula:

(3.1) Zone non-porous:

$$\frac{\partial}{\partial x_i}\left(\rho_f c p_f u_i T\right) = \frac{\partial}{\partial x_i}\left[(\frac{\mu}{Pr} + \frac{\mu_t}{\sigma_T})\frac{\partial}{\partial x_i}(\frac{\lambda_f}{\rho_f c p_f}T)\right] \qquad (4)$$

(3.2) Porous region:

For Fluid:

$$\frac{\partial}{\partial x_j}\left(\lambda_{f,eff}\frac{\partial T_f}{\partial x_j}\right) = \rho_f c p_f u_i \frac{\partial T_f}{\partial x_i} \qquad (5)$$

For Solid:

$$\frac{\partial}{\partial x_j}\left(\lambda_{s,eff}\frac{\partial T_f}{\partial x_j}\right) = 0 \qquad (6)$$

where solids are denoted by s, fluid surfaces by f, and thermal expansion coefficients and conductivity by cp and λ. Metal foam's porosity (φ), permeability (K), and inertia coefficient (F), which can be expressed as follows:

$$K = 0.00073(1-\varphi)^{-0.224} - \left(\frac{d_f}{d_p}\right)^{-1.11} d_p^2 \qquad (7)$$

$$F = 0.00212(1-\varphi)^{-0.132}(\frac{d_f}{d_p})^{-1.63} \qquad (8)$$

The dimensions given are the diameter of the pore and the diameter of the metal fiber, which are provided as:

$$d_p = \frac{0.0254}{\omega} \qquad (9)$$

$$\frac{d_f}{d_p} = 1.18\sqrt{\frac{1-\varphi}{3\pi}}\left(\frac{1}{1-e^{-(1-\varphi)/0.04}}\right) \qquad (10)$$

The model's obtained equations are used to compute the effective thermal conductivity.

$$d = \sqrt{\frac{\sqrt{2}(2-(\frac{5}{8})e^3\sqrt{2}-2\varepsilon)}{\pi(3-4e\sqrt{2}-e)}} \quad (11)$$

$$R_A = \frac{4d}{(2e^2+\pi d(1-e))k_s+(4-2e^2-\pi d(1-e))\lambda_f} \quad (12)$$

$$R_B = \frac{(e-2d)^2}{(e-2d)e^2k_s+(2e-4d-(e-2d)e^2)\lambda_f} \quad (13)$$

$$R_C = \frac{(\sqrt{2}-2e)^2}{2\pi d^2(1-2e\sqrt{2})k_s+2(\sqrt{2}-2e-\pi d^2(1-2e\sqrt{2}))\lambda_f} \quad (14)$$

$$R_D = \frac{2e}{e^2k_s+(4-e^2)\lambda_f} \quad (15)$$

$$k_{eff} = \frac{\sqrt{2}}{2(R_A+R_B+R_C+R_D)} \quad (16)$$

Turbulent flows are analyzed using the conventional $k-\epsilon$ model. The physical equations for turbulence kinetic energy (k) and dissipation rate (ϵ) are shown below:

$$\frac{\partial}{\partial x_i}(\rho u_i k) = \frac{\partial}{\partial x_i}\left[(\mu + \frac{\mu_t}{\sigma_k})\frac{\partial k}{\partial x_i}\right] + G_k - \rho\epsilon \quad (17)$$

$$\frac{\partial}{\partial x_i}(\rho u_i \epsilon) = \frac{\partial}{\partial x_i}\left[(\mu + \frac{\mu_t}{\sigma_\epsilon})\frac{\partial k}{\partial x_i}\right] + C_{1\epsilon}\frac{\epsilon}{k}G_k - C_{2\epsilon}\rho\frac{\epsilon^2}{k} \quad (18)$$

where $C_{1\epsilon}$, $C_{2\epsilon}$, C_μ, σ_K, and σ_ϵ are constants. These constants are 1.44, 1.92, 0.09, 1.0, and 1.3, respectively. G_k and μ_t are the disturbance kinetic energy and turbulent viscosity, respectively. Their values are determined based on the generation they represent, as follows:

$$G_k = \mu_t \frac{\partial u_j}{\partial x_i}\left(\frac{\partial u_i}{\partial x_j} + \frac{\partial u_j}{\partial x_i}\right) \quad (19)$$

$$\mu_t = \rho C_\mu \frac{k^2}{\varepsilon} \quad (20)$$

2.4.Boundary Conditions

The inside wall of the absorber pipe and the exterior of the metallic structure conform to the no-slip requirement, and turbulent variables are handled using the wall function method. Figure 2 shows more comprehensive boundary conditions:

1) Inlet: unified flow and temperature settings,
   $u_x = u_y = 0, u_z = u_i, T = T_i = 298.15\ k$
2) Outlet: outflow and fully-developed assumption,
   $\frac{\partial u_i}{\partial z} = \frac{\partial T}{\partial z} = \frac{\partial p}{\partial z} = 0$
3) Outer Walls: The pipe walls were divided into two parts: the top wall, exposed to direct solar flux, and the bottom wall, which received radiation from the parabolic reflector aimed at the PTC mirror. The uneven heat distribution on the outer surface of the absorber tube was determined through Monte Carlo ray tracing in SolTrace.

The ray trace solution has links to the CFD system via translated custom functions. For easier execution of the CFD approach, a heat flow pattern was used as a thermally restrictive condition on the recipient's absorber pipe using regression techniques. Figures 3 and 4 show the arrangement of solar heat flux around the outside wall of the receiver pipe. An irregular heat flow pattern around the receiver's absorber pipe was studied. Lower levels of direct radiation in comparison to reflection cause higher concentrations of heat in the lower area facing the PTC mirror and lower heat flux density in the top section.

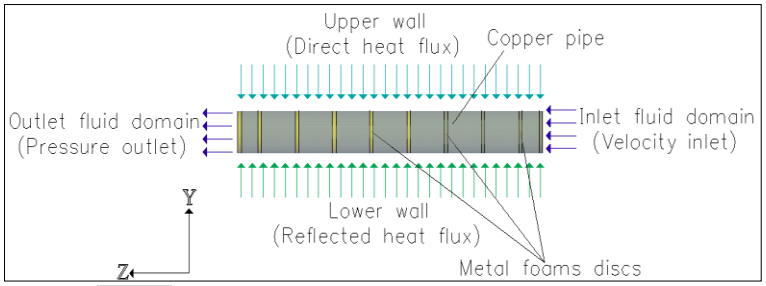

Fig. 2 Boundary Conditions of the Used Models.

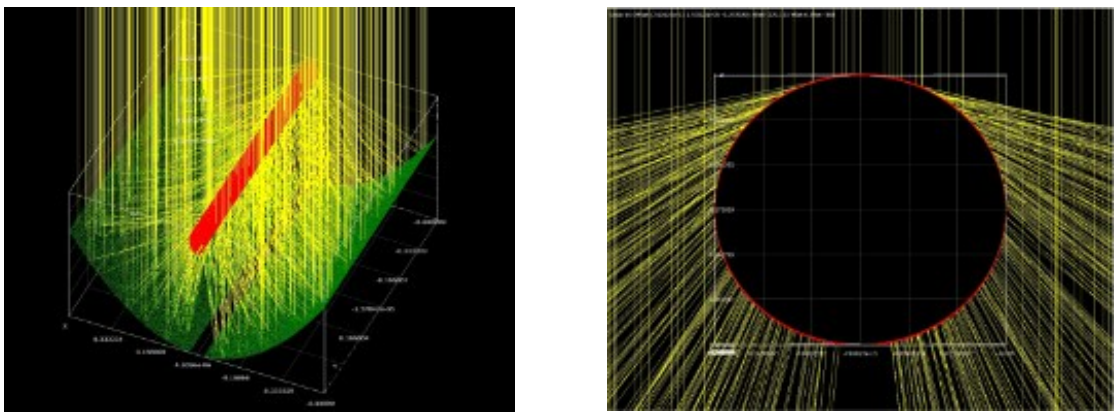

(a) **(b)**

Fig. 3 Ray Tracing: (a) Parabolic Reflector Surface, (b) Contour of the Absorber Tube Surface.

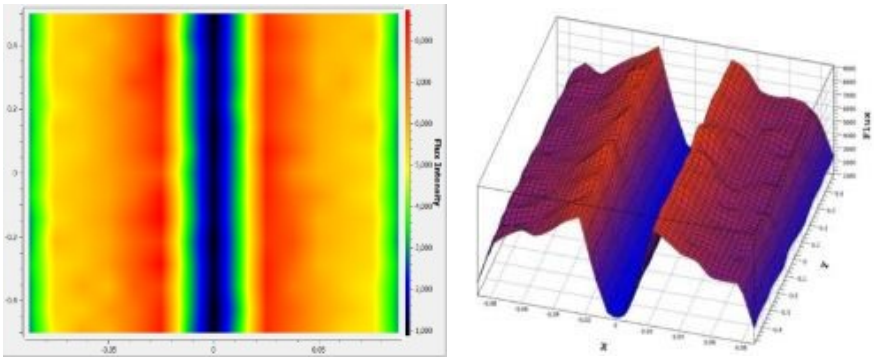

Fig. 4 Three-Dimensional View of the Heat Flux Distribution on the Absorber Tube Surface.

3.NUMERICAL PROCEDURE

The equations governing the system were discretized using a finite volume method. Custom functions were employed to enforce non-uniform heat flux boundary conditions. Pressure and velocity were coupled using a straightforward approach. A second-order upwind approach was used to account for convective effects in momentum, turbulence kinetic energy, dissipation rates, temperature variations, and energy equations. Confluence is obtained if the scaled residuals of the energy equation fall below 10^{-8}; however, other variables must be less than 10^{-6}. A grid-independent study was conducted to assess the accuracy of the numerical solution. The optimal mesh size was identified by examining grid sizes ranging from 161,437 to 1,640,304 elements. The findings indicated that a mesh size of 1,640,304 elements exhibited minimal temperature fluctuations compared to finer grids while maintaining computational efficiency, as depicted in Fig. 5. To accurately capture complex flow behavior in the metal foam regions, a more detailed meshing approach using an irregular array in the z-axis was developed. Convergence required achieving a relative error of less than 10^{-8}. For the joint velocity and temperature domain, which undergoes consecutive repetitions, the remainder was normalized for the pressure domain.

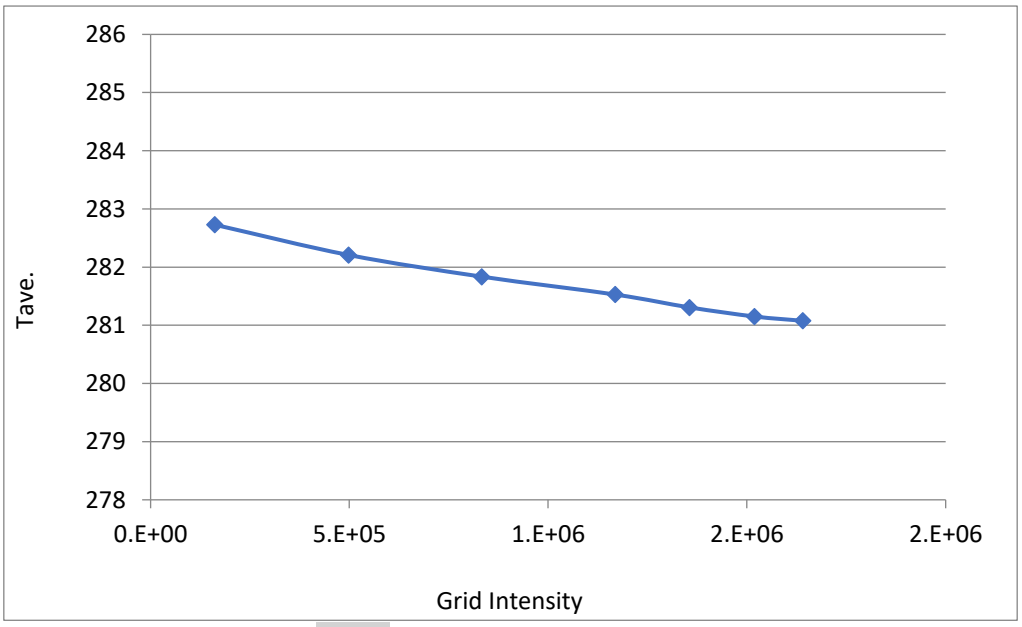

Fig. 5 Grid Independence Curve.

4.VERIFICATION OF CODE

The program codes were verified by comparing numerical outcomes with those from previous studies [8, 10]. Figure 6 compares friction factors versus Reynolds numbers for different metal foam designs in the receiver tube. The inclusion of metal foam led to a significant increase in the friction factor at equivalent Reynolds numbers. Additionally, the influence of various metal foam configurations on the temperature difference and thermal efficiency of a direct absorption PTC was examined across varying flow rates. As shown in Fig. 7, the temperature difference of the HTF decreased gradually as the HTF flow rate increased. Moreover, Fig. 8 indicates that the thermal efficiency increased with flow rate at constant inlet temperature. A comparative analysis of these research findings and those offered by [8, 10] reveals that the code used in the present study displayed good reliability and precision.

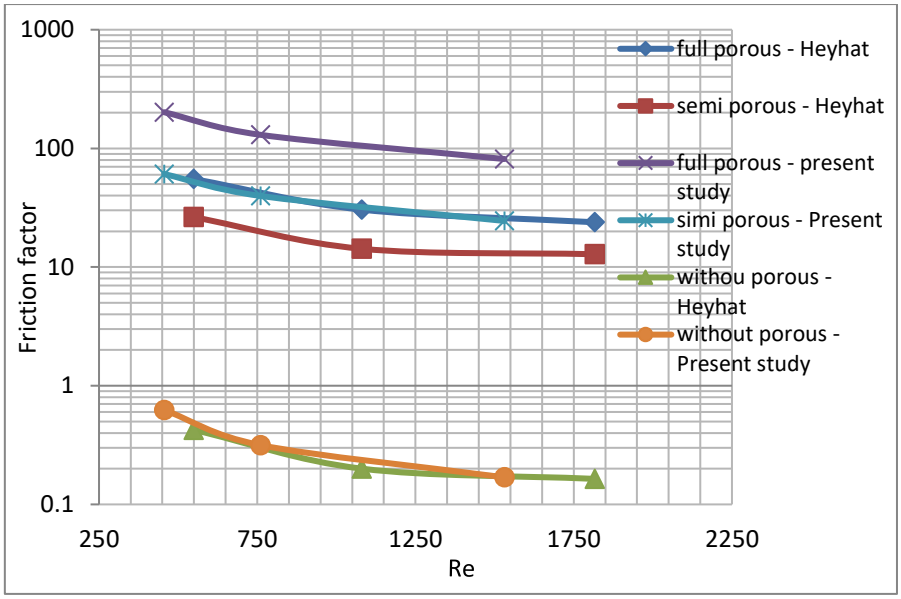

Fig. 6 The Variation of the Friction Factor in Different Configurations of Porous Foams with Reynolds Number.

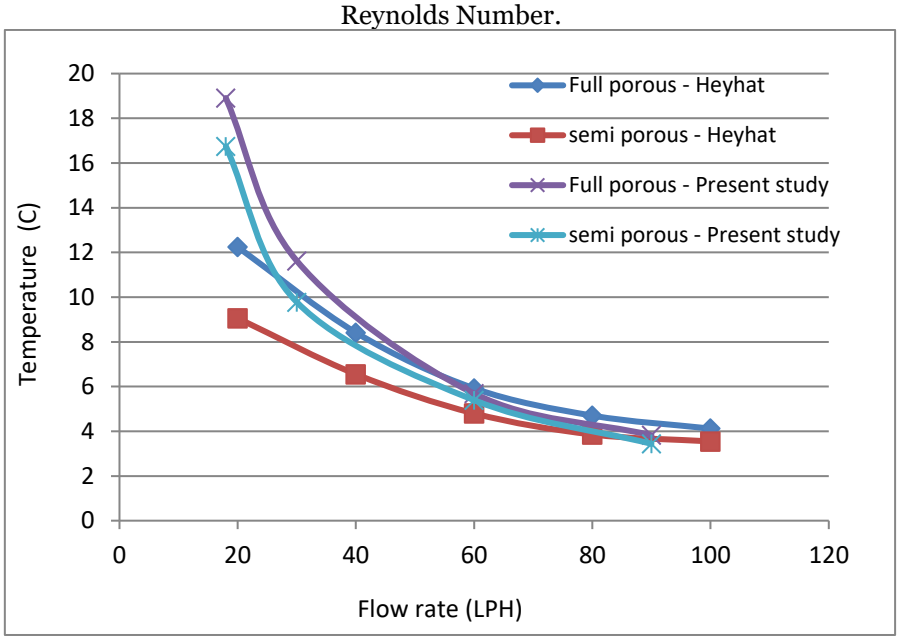

Fig. 7 The Variation of Temperatures at Different Flow Rates and Configurations of the Metal Foam Receiver.

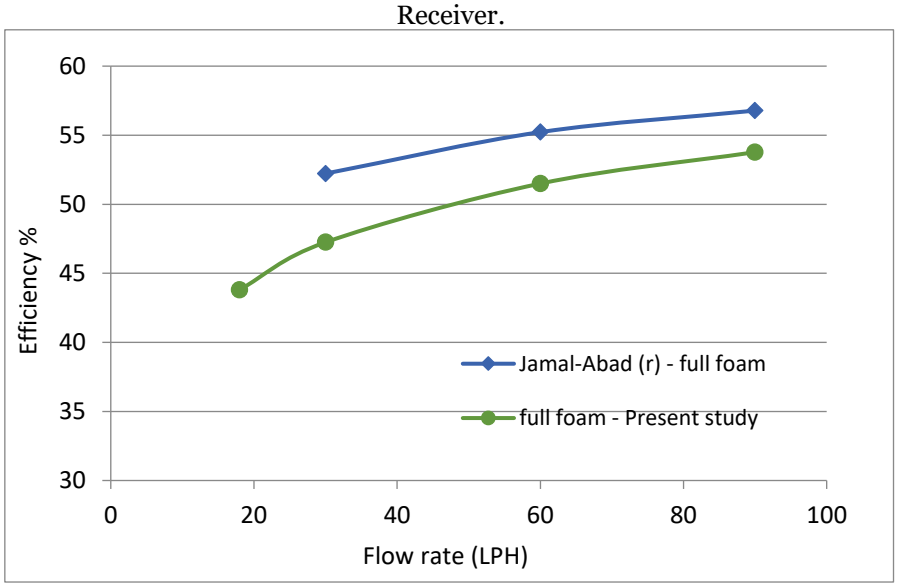

Fig. 8 Comparison of Thermal Efficiency of Using Metal Foam in PTC at different Flow Rates.

5.RESULTS AND DISCUSSION

The influence of the absorber with MFI on the performance of PTC was investigated. The inclusion of copper foam improved the thermal conductivity of the adsorbent, and therefore, the power capable of transmitting heat from the surface to the water was increased. Ref. [21] investigated the efficient heat transfer of metal foam. The tests were conducted on a 1.5 m long absorber pipe with a diameter of 26 mm. The absorber pipe held ten copper foam blocks, each measuring 45 mm in thickness, resulting in a filling ratio of 30%. The copper foam had a porosity value ε of 0.8981, an inertial coefficient C of 0.16, a permeability K of 1.75 x 10^{-8}, and a pore density of 40 PPI. Water was used as a working fluid. Numerical outputs include pressure drops, temperature distributions, streamlines, and parameters for heat transfer at a specific location

5.1.Decrease in Pressure

Figure 9 shows the impact of MFI blocks on the distribution of pressure within the pipe. The MFI caused a greater pressure drop than when only fluid was present, attributed to the permeability and sinuous routes within the porous structure of the metal foam. Furthermore, Fig. 9 indicates a linear decline in pressure across the metal foam blocks, likely due to low HTF velocity in the pipe.

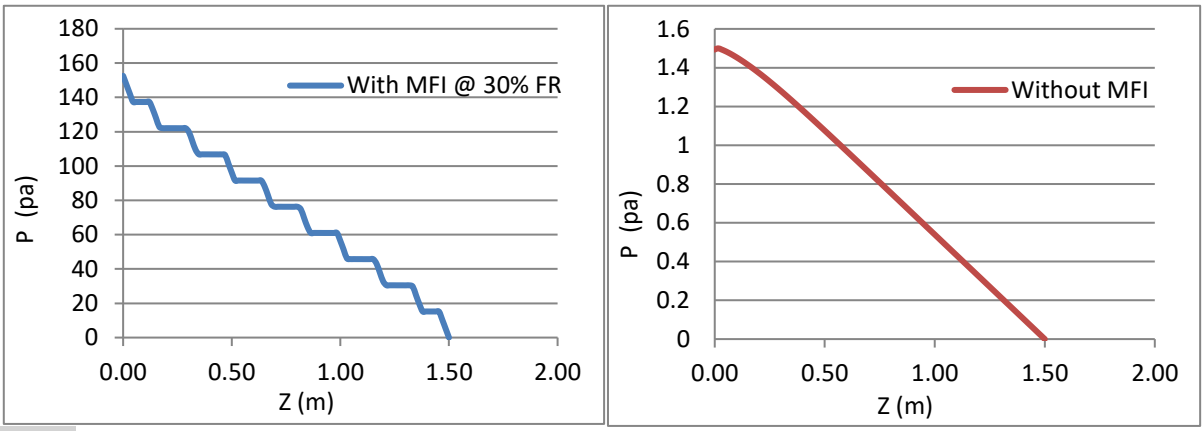

Fig. 9 Local Pressure Distribution Along the PTR with and without MFI for Re =455.855 and FR 30%.

5.2.Distribution of Temperature

Overall, metal foam blocks disrupt the formation of the boundary layer across the pipe. Additionally, fluid passing through metal foam blocks plays a significant role in disrupting the formation of thermal boundary layers across the pipe, as well as disturbing the development of subsequent thermal boundary layers. Figures 10, 11, 12, and 13 show the impact of placing MFI in the pipe on temperature distribution. The MFI blocks significantly decreased the wall temperature, while they significantly increased the HTF temperature. This enhancement in heat transfer is attributed to some heat being conducted through the solid matrix from the heat source, while convection facilitates its transfer to the incoming fluid. Figs. 10 and 11 show the temperature patterns around the pipe with and without MFI, respectively, under different levels of radiation from the sun. Solar radiation readings were captured at noon (869 W/m²) and in the late afternoon (596 W/m²). The temperature patterns along the pipe seem to remain largely unaffected by variations in solar radiation intensity. This lack of noticeable influence may be due to factors like the composition of the working fluid and limitations linked to fluctuations in the strength of solar radiation. Figures 12 and 13 show the impact of different Re numbers on the formation of the thermal boundary layer at a constant solar radiation intensity (I=869 W/m²). There is an inverse relationship between temperature and Re number values. The increase in Re numbers reduced the thermal boundary layer formation, indicating enhanced fluid mixing and decreased thickness of the thermal boundary layer.

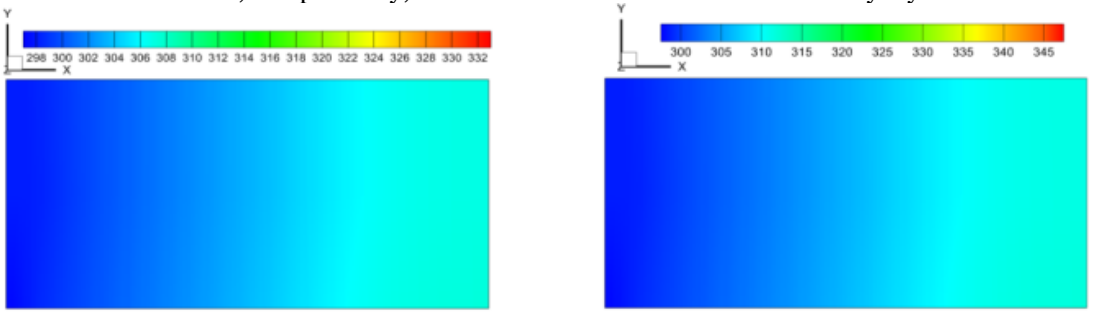

(a) **(b)**

Fig. 10 Temperature Contours for the Channel without MFI for Different Solar Radiation Intensity and Re=455.855, (a) I=596 W/m², (b) I=869 W/m².

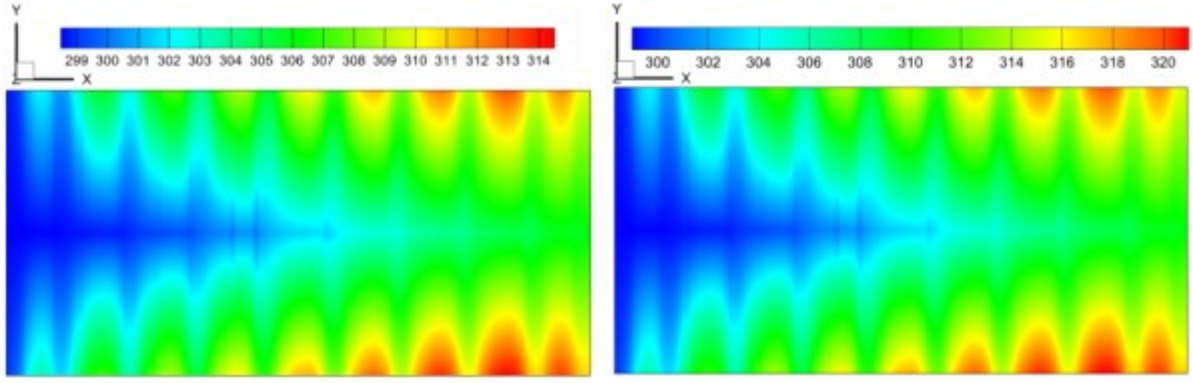

(a) **(b)**

Fig. 11 Temperature Contours for the Channel with MFI for Different Solar Radiation Intensity and Re=455.855, (a) I=596 W/m², (b) I=869 W/m².

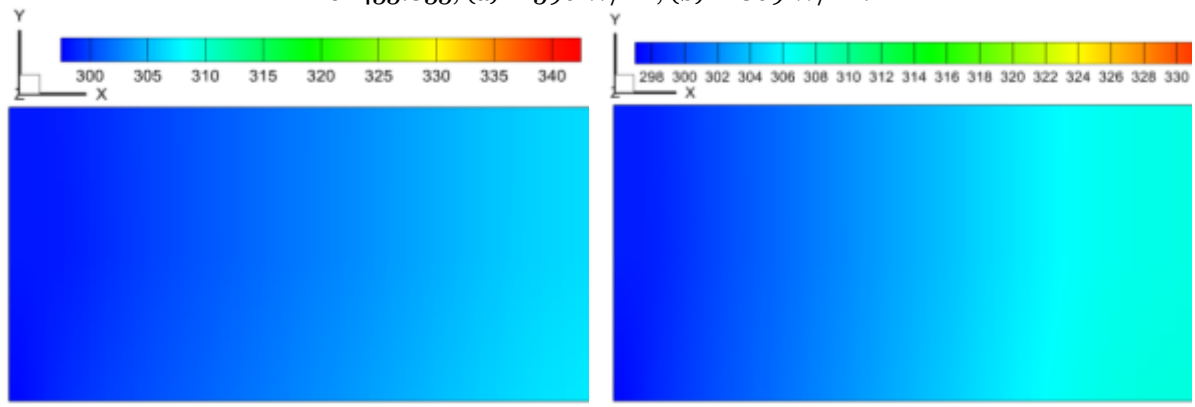

(a) **(b)**

Fig. 12 Temperature Contours for the Channel without MFI with (a) Re =455.855, (b) Re = 760.566.

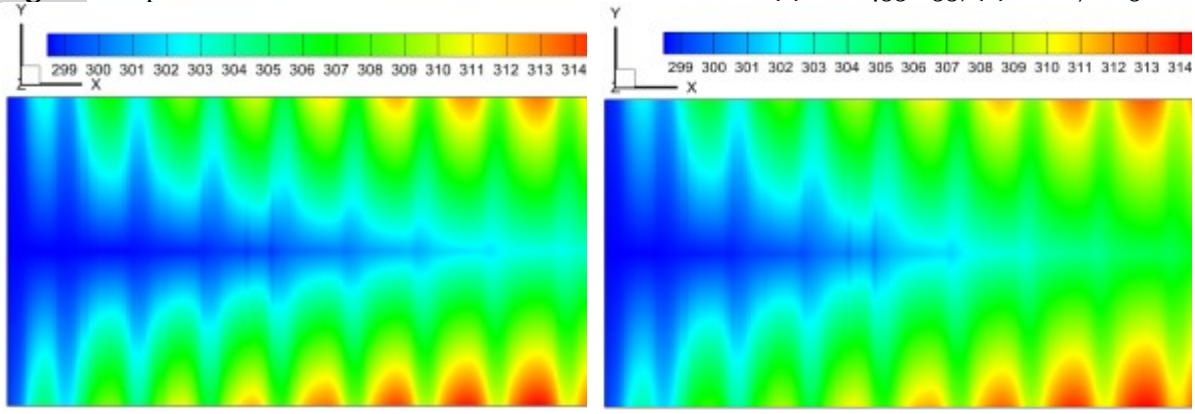

(a) **(b)**

Fig. 13 Temperature Contours for the Channel without MFI with (a) Re =455.855, (b) Re = 760.566.

5.3.Heat Transfer Coefficient

Figure 14 shows the local heat transfer coefficient along the absorber pipe of a PTC without MFI. The coefficient decreased as the flow progressed downstream. Near the pipe's inlet, the thermal boundary layer was thin, and the temperature differential between the water and the surface was high, resulting in a high local heat transfer coefficient. As the fluid moved downstream, the thermal boundary layer thickened, lowering the temperature gradient and the local heat transfer coefficient. The observed drop in the local heat transfer coefficient is caused by the continual growth of the thermal boundary layer as a result of continued heating, which reduces the temperature differential between the water and the surface pipe. Figure 14 shows that the PTC with MFI had a larger coefficient of heat transfer with time than the collector without MFI. This enhancement is due to the disruption of the thermal boundary layer and increased surface area for heat exchange, which results in more efficient heat transfer. With MFI, metal foam blocks break the boundary layer, preventing it from thickening and maintaining a high-temperature distinction between the water and the surface. MFI caused disruptions in fluid flow, which improved convective heat transfer by constantly mixing the fluid and ensuring that cooler fluid contacts the hot surface. This disturbance disrupted the thermal

boundary layer, allowing for a larger heat transfer coefficient along the absorber pipe's length. Metal foam's ability to conduct heat through its solid matrix while promoting effective fluid convection contributes to the observed higher heat transfer rates.

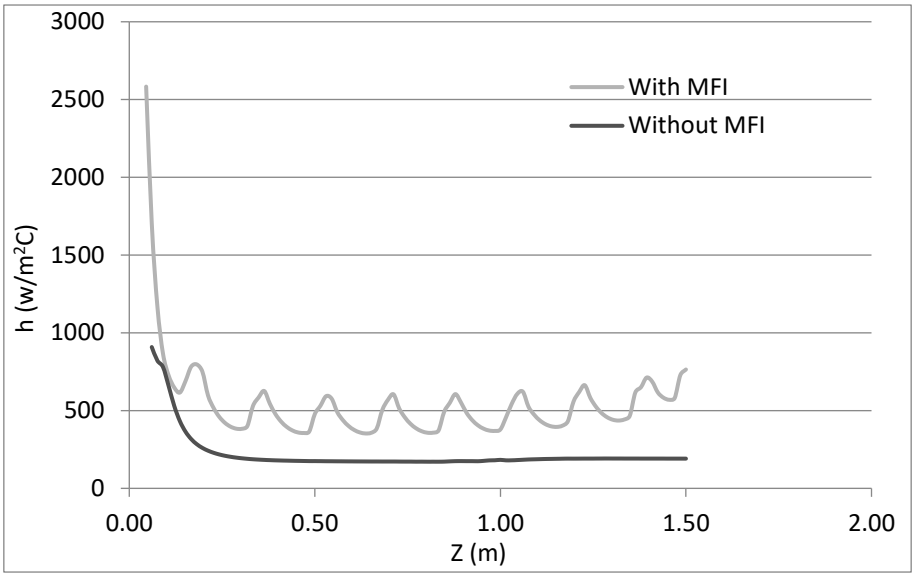

Fig. 14 Local Convection Heat Transfer Coefficient Distribution Along the Pipe with and Without MFI for 0.3 LPM Flow Rates.

Figure 15 shows how adding metal foam pieces can improve the average convective heat transfer coefficient over a range of data and collector water flow rates. It is evident that at a high volume water flow rate, the heat transfer ratio increased to its maximum amount. This behavior occurs because the thermal boundary layer thickness is inversely proportional to the fluid flow rate, leading to an increase in the improvement of the heat transfer coefficients as the volume of water flow rate increases.

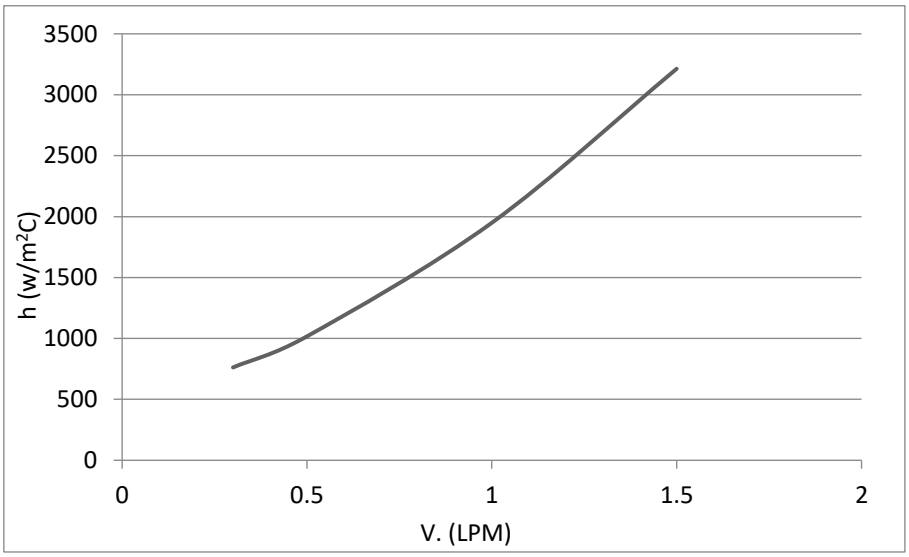

Fig. 15 Variations in the Mean Convection Heat Transfer Coefficient with 30% FR MFI at Varying Water Flow Rates.

5.4.A Comparison of Metal Foam Configurations in Partial and Full

Figure 16 highlights two key aspects of metal foam configurations in a PTC: T_{out} and Δp generated by fluid flow. The average outlet temperature (T_{out}) in the partial metal foam configuration was approximately 33.8°C, which is sufficient for many applications depending on the system's required operating temperatures. This value was lower than in the full metal foam configuration. The pressure drop (Δp) for this configuration was around 500 Pa, significantly lower than that of the fully packed configuration. This decrease in pressure drop indicates reduced resistance to fluid flow, allowing the working fluid (water) to circulate more easily. As a result, low-power pumps are sufficient, reducing energy consumption and operational costs associated with fluid circulation. In comparison, the totally metal foam had a higher exit temperature of approximately 34.9°C, indicating better heat

transfer. The metal foam's increased surface area boosts heat absorption from the solar collector, making it useful for applications requiring higher output temperatures. However, this configuration resulted in a much higher pressure drop, over 2000 Pa, indicating strong resistance to fluid movement. To maintain the needed flow rate, more powerful pumps are required, increasing energy consumption and operational costs. While higher outlet temperatures improve thermal efficiency, the huge pressure drop creates a trade-off, since the increased energy required to circulate the fluid may outweigh the thermal benefits, especially in systems that operate for more extended periods of time or at higher flow rates. Partial metal foam construction strikes a balance between moderate heat transfer (lower T_{out}) and low running costs (low-pressure drop), making it suitable for situations where energy efficiency is more important than achieving maximum temperature. The filled metal foam configuration, on the other hand, maximized thermal performance (higher T_{out}) while incurring significantly higher energy costs due to increased pressure drop, making it ideal for applications that require high outlet temperatures at the expense of increased operational investment. To summarize, the system's particular requirements dictate whether to use partial or whole metal foam arrangements. Partial metal foam is desirable for systems that prioritize energy efficiency and low operational costs; however, filled metal foam is better suited for applications requiring maximal heat transfer, despite higher pumping power requirements and associated operational costs.

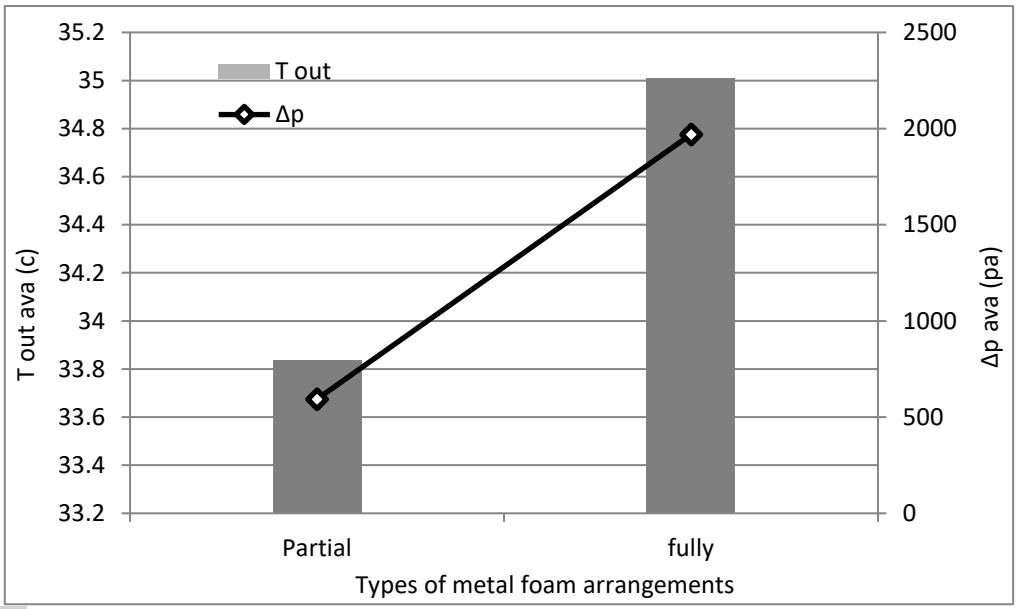

Fig. 16 Variation of Average Outlet Water Temperature and Pressure Drop of PTC with Different Arrangements of Copper Metal Foam.

5.5.Impact of MFI on PTC Efficiency

Figure 17 shows the effect of different volume flow rates on the efficiency of PTC. In any case, raising flow rates improves efficiency. The collector without MFI had the lowest efficiency across the range, starting above 40% at 0.3 LPM and increasing to 42% at 1.5 LPM, indicating lowered constraints to the fluid's ability to absorb heat. In comparison, the partial MFI at 30% FR performs significantly better, with efficiency increasing from 44% at 0.3 LPM to 48% at 1.5 LPM. This behavior shows that even partial MFI promotes heat transfer by increasing surface area and allowing for better fluid mixing. The full MFI achieves the highest efficiency, starting at 46% at 0.3 LPM and exceeding 52% at 1.5 LPM. The data indicated that both partial and full MFI significantly improved heat transfer in PTCs. However, while full foam was the most efficient, it can result in significant pressure loss, as shown in Fig. 16, which must be balanced against pumping power and operational costs.

5.6.The Performance Evaluation Criteria (PEC)

Figure 18 shows a decline in PEC as the flow rate increases, from a low flow rate to a decrease at higher rates. This drop is due to the pressure rise outpacing heat transfer improvements. While higher flow rates boost heat transfer, the increased pressure drop reduces overall efficiency, highlighting the need to balance flow rates for optimal performance.

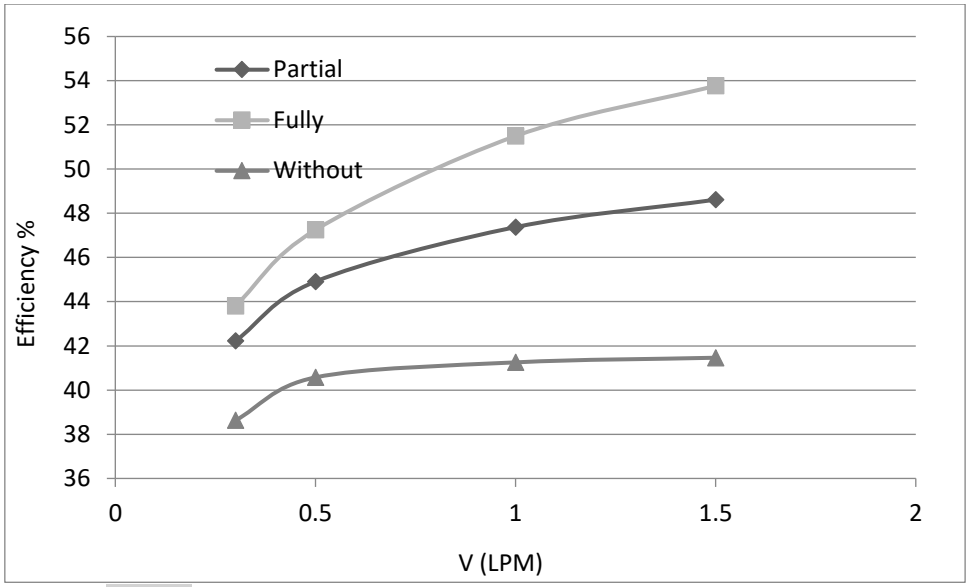

Fig. 17 Average Daily Thermal Efficiency at Varying Flow Rates.

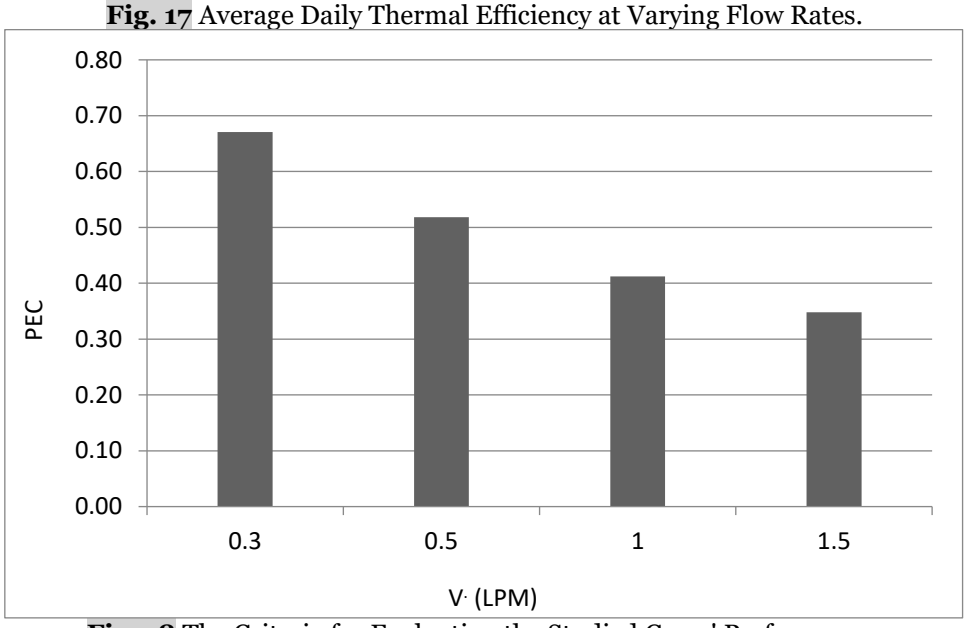

Fig. 18 The Criteria for Evaluating the Studied Cases' Performance.

6.CONCLUSIONS

The main findings of the present work can be summarized as follows:

1) The temperature of the fluid was high when the metal foam blocks were inserted, compared to the case without metal foam blocks.
2) When a PTC tube was partially filled with metal foam instead of being empty, it exhibited a more uniform temperature variation on the exterior wall surface and a smaller variation between the highest and lowest temperatures. This behavior shows that employing metal foam may decrease heat stress and enhance the protection of the PTC system. MFI improved heat transfer properties and reduced heat flux fluctuations.
3) As the Re number increased, both the local and average heat transfer coefficients also increased.
4) The addition of MFI raised the average heat transfer coefficient by more than 80% compared to a situation with only fluid.
5) Replacing an empty pipe with MFI enhanced the thermal-hydraulic and thermodynamic efficiency of the PTC tube.
6) The use of metal foam blocks significantly enhanced heat transfer in the PTC tube, resulting in a 42% to 96% rise in the Nusselt numbers. However, it also increased flow resistance, with the friction factor (f) ranging from 54 to 96 times that of an empty tube. The PEC changed and lowered with increasing Re number, showing that metal foam blocks significantly improved the overall thermal-hydraulic performance of the PTC pipe, particularly at lower Re values.

ACKNOWLEDGEMENTS

The authors are grateful for the support of this research provided by the Mechanical Engineering Department, College of Engineering, Baghdad University. Postgraduate Research No.1197 at 15-6-2020.

NOMENCLATURE

C	Inertial Coefficient
Cp	Specific heat at constant pressure, J/kg.K
Da	Darcy number
Dh	Hydraulic diameter, m
FR	Filling Ratio,
h	Heat transfer coefficient, W/m².K
I	Solar intensity on horizontal surface, W/m²
λ	Thermal conductivity, W/(m K)
K	Permeability, m²
Nu	Local Nusselt Number,
p	Pressure, Pa
Pr	Prandtl Number,
Re	Reynolds Number,
T	Temperature, °C
u	Velocity component in x-direction, m/s
U	Heat loss coefficient, W/m². °C
V˙	Volumetric flow rate, LPM
Greek Symbols	
α	Absorptivity
*(α τ)*e	Effective transmittance
ε	Porosity, Emissivity
η	Thermal efficiency, %
λ	Thermal conductivity ratio
μ	Dynamic viscosity, kg m/s
υ	Kinetic viscosity, m²/s
ρ	Density, kg/m³
σ	Stefan – Boltzmann constant, W/m².K⁴
τ	Transmissivity
Subscripts	
f	Fluid
i	Inlet
o	Outlet
LTE	Local Thermal Equilibrium
LPM	Liter Per Minute
MFI	Metal Foam Insertion
PPI	Pore Per Inch
PTC	Parabolic trough collector
HTF	Heat transfer fluid

REFERENCES

[1] Ashby MF, Evans AG, Fleck NA, Gibson LJ, Hutchinson JW, Wadley HNG. **Metal Foams: A Design Guide**. 1st Edition, Boston, USA: Butterworth-Heinemann; 2000.

[2] Al-Nimar MK, Alkam MK. **Solar Collectors with Tubes Partially Filled with Porous Substrate**. *ASME Journal of Solar Energy Engineering* 1999; **121**(1): 20–24.

[3] Ravi Kumar K, Reddy KS. **Effect of Porous Disc Receiver Configurations on Performance of Solar Parabolic Trough Concentrator**. *Heat and Mass Transfer* 2012; **48**(4): 555–571.

[4] Kumar KR, Reddy KS. **Thermal Analysis of Solar Parabolic Trough with Porous Disc Receiver**. *Applied Energy* 2009; **86**(9): 1804–1812.

[5] Mwesigye A, Bello-Ochende T, Meyer JP. **Heat Transfer and Thermodynamic Performance of a Parabolic Trough Receiver with Centrally Placed Perforated Plate Inserts**. *Applied Energy* 2014; **136**: 989–1003.

[6] Wang P, Liu DY, Xu C. **Numerical Study of Heat Transfer Enhancement in the Receiver Tube of Direct Steam Generation with Parabolic Trough By Inserting Metal Foams**. *Applied Energy* 2013; **102**: 449–460.

[7] Zheng ZJ, Xu Y, He YL. **Thermal Analysis of a Solar Parabolic Trough Receiver Tube with Porous Insert Optimized By Coupling Genetic Algorithm and CFD**. *Science China-Technological Sciences* 2016; **59**(10): 1475–1485.

[8] Jamal-Abad MT, Saedodin S, Aminy M. **Experimental Investigation on A Solar Parabolic Trough Collector For Absorber Tube Filled with Porous Media**. *Renewable Energy* 2017; **107**: 156–163.

[9] Heyhat MM, Valizade M, Abdolahzade Sh, Maerefat M. **Thermal Efficiency Enhancement of Direct Absorption Parabolic Trough Solar Collector (DAPTSC) By Using Nanofluid and Metal Foam**. *Energy* 2020; **192**: 116662.

[10] Valizade M, Heyhat MM, Maerefat M. **Experimental Study of the Thermal Behavior of Direct Absorption Parabolic Trough Collector By Applying Copper Metal Foam As Volumetric Solar Absorption**. *Renewable Energy* 2020; **145**: 261–269.

[11] Peng H, Li M, Liang X. **Thermal-Hydraulic and Thermodynamic Performance of Parabolic Trough Solar Receiver Partially Filled with Gradient Metal Foam**. *Energy* 2020; **211**: 119046.

[12] Peng H, Li M, Hu F, Feng S. **Performance Analysis of Receiver Pipe in Parabolic Trough Solar Collector Inserted with Semi-Annular and Fin Shape Metal Foam Hybrid Structure**. *Case Studies in Thermal Engineering* 2021; **26**: 101112.

[13] Helmi N, Nazari A, Bezaatpour M, Nateghi S, Ghaebi H. **Investigation of Energy Storage in Parabolic Rotary Trough Solar Collectors Using Various Porous Fins with Magnetic Nanoparticles**. *Energy for Sustainable Development* 2022; **70**: 194–204.

[14] Esmaeili Z, Akbarzadeh S, Rashidi S, Valipour MS. **Effects of Hybrid Nanofluids and Turbulator on Efficiency Improvement of Parabolic Trough Solar Collectors**. *Engineering Analysis with Boundary Elements* 2023; **148**: 114–125.

[15] Heyhat MM, Zahi Khattar M. **On the Effect of Different Placement Schemes of Metal Foam as Volumetric Receiver on the Thermal Performance of a Direct Absorption Parabolic Trough Solar Collector**. *Energy* 2023; **266**: 126428.

[16] Esmaeili Z, Valipour MS, Rashidi S, Akbarzadeh S. **Performance Analysis of a Parabolic Trough Collector Using Partial Metal Foam Inside an Receiver Pipe: An Experimental Study**. *Environmental Science and Pollution Research* 2023; **30**(4): 89794–89804.

[17] Farhan IS, Mohammed AA, Al-Jethelah MS. **The Effect of Uneven Metal Foam Distribution on Solar Compound Parabolic Trough Collector Receiver Thermal Performance**. *Tikrit Journal of Engineering Sciences* 2024; **31**(1): 291–305.

[18] Rabbani P, Hamzehpour A, Ashjaee M, Najafi M, Houshfar E. **Experimental Investigation on Heat Transfer of Mgo Nanofluid in Tubes Partially Filled with Metal Foam**. *Powder Technology* 2019; **354**: 734–742.

[19] Li YZ, Wang SX, Zhao YL. **Experimental Study on Heat Transfer Enhancement of Gas Tube Partially Filled with Metal Foam**. *Experimental Thermal and Fluid Science* 2018; **97**: 408–416.

[20] Chen CC, Huang PC. **Numerical Study of Heat Transfer Enhancement for A Novel Flat-Plate Solar Water Collector Using Metal-Foam Blocks**. *International Journal of Heat and Mass Transfer* 2012; **55**(23–24): 6734–6756.

[21] Boomsma K, Poulikakos D. **On The Effective Thermal Conductivity of A Three-Dimensionally Structured Fluid-Saturated Metal Foam**. *International Journal of Heat and Mass Transfer* 2001; **44**(4): 827–836.